



UNIVERSITY OF LEEDS

This is a repository copy of *Development of an efficient, low-operating-pressure graphene oxide / polyethersulfone nanofiltration membrane for removing various water contaminants*.

White Rose Research Online URL for this paper:

<https://eprints.whiterose.ac.uk/210213/>

Version: Accepted Version

---

**Article:**

Elessawy, N A, Exley, J, El-Sayed, D S et al. (5 more authors) (2024) Development of an efficient, low-operating-pressure graphene oxide / polyethersulfone nanofiltration membrane for removing various water contaminants. *Journal of Environmental Chemical Engineering*, 12 (2). 112489. ISSN 2213-3437

<https://doi.org/10.1016/j.jece.2024.112489>

---

© 2024, Elsevier. This manuscript version is made available under the CC-BY-NC-ND 4.0 license <http://creativecommons.org/licenses/by-nc-nd/4.0/>. This is an author produced version of an article published in the *Journal of Environmental Chemical Engineering* Uploaded in accordance with the publisher's self-archiving policy.

**Reuse**

This article is distributed under the terms of the Creative Commons Attribution-NonCommercial-NoDerivs (CC BY-NC-ND) licence. This licence only allows you to download this work and share it with others as long as you credit the authors, but you can't change the article in any way or use it commercially. More information and the full terms of the licence here: <https://creativecommons.org/licenses/>

**Takedown**

If you consider content in White Rose Research Online to be in breach of UK law, please notify us by emailing [eprints@whiterose.ac.uk](mailto:eprints@whiterose.ac.uk) including the URL of the record and the reason for the withdrawal request.



[eprints@whiterose.ac.uk](mailto:eprints@whiterose.ac.uk)  
<https://eprints.whiterose.ac.uk/>

# **Development of an efficient, low-operating-pressure graphene oxide / polyethersulfone nanofiltration membrane for removing various water contaminants**

Noha A. Elessawy<sup>a,\*</sup>, James Exley<sup>b</sup>, Doaa S. El-Sayed<sup>c</sup>, Arafat Toghan<sup>d, e</sup>, Sami A. Al-Hussain<sup>d</sup>, Mohamed Elzokm<sup>f</sup>, Abdelaziz H. Konsowa<sup>g</sup>, Martin Tillotson<sup>b</sup>

<sup>a</sup> Computer Based Engineering Applications Department, Informatics Research Institute, New Borg El-Arab City 21934, Alexandria, Egypt.

<sup>b</sup> School of Civil Engineering, University of Leeds, Leeds, West Yorkshire, LS2 9JT, UK

<sup>c</sup> Chemistry Department, Faculty of Science, Alexandria University, Alexandria 21511, Egypt

<sup>d</sup> Chemistry Department, College of Science, Imam Mohammad Ibn Saud Islamic University (IMSIU), Riyadh 11623, Saudi Arabia

<sup>e</sup> Chemistry Department, Faculty of Science, South Valley University, Qena 83523, Egypt.

<sup>f</sup> Pearl GTL Laboratory, Technology Department, Qatar Shell GTL, 3747 Ras Laffan, Qatar

<sup>g</sup> Chemical Engineering Department, Faculty of Engineering, Alexandria University, Alexandria, Egypt

corresponding-author: [nony\\_essawy@yahoo.com](mailto:nony_essawy@yahoo.com) (Noha A. Elessawy) , [arafat.toghan@yahoo.com](mailto:arafat.toghan@yahoo.com);

[aatahmed@imamu.edu.sa](mailto:aatahmed@imamu.edu.sa) (Arafat Toghan)

## **Abstract**

Conventional wastewater treatment technologies tend to be high-capex, energy-intensive solutions that lack specificity for different pollution classes, and do not lend themselves to wide-scale deployment, particularly in areas of the world where industrial wastewater discharge is a significant environmental problem. In tandem, solid waste pollution arising, particularly plastic containing waste, is a persistent and serious pollution issue. This work focuses on the concept of "waste treating waste" and a multidisciplinary effort ranging from materials science and environmental management to sustainable water treatment, in addition to production of graphene

oxide from mineral water waste bottles using a simple synthetic procedure that can be economically scaled up for use as a cost-effective adsorbent. Prepared graphene oxide was supported on a polyethersulfone (PES) membrane, and batch filtration studies were performed to examine its performance in the removal of methylene blue (MB) dye, Gentimicin sulphate (GMS) antibiotic, and  $\text{Na}_2\text{SO}_4$  and  $\text{MgSO}_4$  salts from an aqueous solution. Operating parameters such as initial pollutant concentration, time, and solution pH were investigated and optimized using a response surface methodology (RSM) model. The results confirm the significant efficiency of the filtration process, with a maximum rejection of about 91% for MB, 93% for GMS, 67% for  $\text{Na}_2\text{SO}_4$ , and 64% for  $\text{MgSO}_4$ , with maximum water flux of 1322, 1367, 1225, and 1059 LMH, respectively. Density functional theory calculations were considered for the GO, PES membrane, and GO/PES membrane with a GGA/PBE optimization level. Adsorption annealing locator analysis was performed for the GO/PES membrane, and the process was recalculated for MB as adsorbate. In conclusion, the adsorption effect employing produced GO/PES membrane is the most important removal, followed by Donnan exclusion and steric hindrance effect. Therefore, it is possible to build new eco-friendly membranes for nanofiltration that are affordable, stable, and effective in removing various pollutants from water systems.

**Keywords:** nanofiltration, antibiotic removal, dye removal, metal ion removal, graphene oxide, polyethersulfone membrane.

## 1. Introduction

Industrial activity involves the use of many different chemicals, which, if not properly controlled, can be discharged into the aquatic environment. Dyes, pharmaceutical by-products,

and heavy metals are common examples of polluted and harmful chemicals that, if allowed to enter the aquatic environment via industrial wastewater, can poison aquatic life and be harmful to human health. Many treatment techniques have been developed to eliminate these pollutant compounds from wastewater, however they are typically costly to install and/or expensive to operate. Pressure-based membrane processes such as reverse osmosis (RO), ultrafiltration (UF), microfiltration (MF), and nanofiltration (NF) have emerged as the most energy efficient and technologically resilient among all water treatment techniques. Recently, NF technology has increased in demand due to its environmental friendliness, low power consumption and provision of greater rejection of multivalent ions and molecules of organic matter with significantly higher flux [1, 2]. Polymers and ceramic materials are commonly employed to fabricate NF membranes. Nevertheless, polymeric membranes are commonly employed in the manufacture of NF membranes due to their excellent film forming properties, appropriate flexibility, and mechanical strength. Polymers such as cellulose acetate (CA) [3], chitosan (CS) [4], polyamides (PA) [5], polyimides (PI) [6], polyvinylalcohol (PVA) [7], polysulphones (PES) [8], and others [9, 10] are being used in NF membranes fabrication.

Amongst the various polymers used for NF membranes, polyethersulfone (PES) is highly preferred because of its excellent chemical and physical properties, ease of fabrication via phase inversion methods, and compatibility with hydrophilic additives, as stated in previous reports [11, 12]. In addition, it is soluble in popular aprotic organic solvents such as dimethylformamide (DMF), N, N-dimethylacetamide (DMAC), and N-methyl-2-pyrrolidone (NMP). However, the inherent hydrophobicity of PES can cause fouling and limited permeation flux due to hydrophobic interactions between the membrane surface and the solute in the solution feed [13-15]. As a result, there is a critical need to improve membrane features, notably surface

characteristics and pore structure, in order to achieve membranes with superior separation performance, wettability, and longer life.

Recently, several studies have demonstrated that graphene-based materials, including graphene oxide (GO), can be used in membrane filtration processes to remove organic and inorganic pollutants from wastewater [16-18]. GO nanosheets are decorated with many hydrophilic oxygen-containing reactive groups, including carboxyl, hydroxyl, and epoxy, on their basal and edges, which gives GO an extraordinary hydrophilicity character [19]. The deprotonation of the carboxylic groups at the terminal of the GO nanosheets, which renders GO negatively charged, also causes GO to show a notable rejection towards salt ions or organic cation molecules across a broad pH range [20, 21]. When compared to unmodified membranes, it has been discovered that a number of PES membranes treated with GO or rGO show better characteristics, including pure water flow, antifouling, solute rejection, and photodegradation [12, 22].

Many researchers have studied the synthesis of GO using conventional hammering [23, 24] or sophisticated electrochemical and microbial techniques [25]. Even that graphene synthesis from plastic waste used complex and expensive techniques [26 - 29]. In this study, we report on our attempts to find a practical solution for plastic waste accumulation and water pollution that can be used on an industrial scale. In other words, waste-derived materials can be used in waste water treatment based on the “wastes-treat-wastes” principle to achieve the goals of waste management and water treatment with cost consideration. By using waste water bottles as low-value waste materials, GO was prepared using the catalytic thermal dissociation technique under autogenic conditions. The prepared GO was deposited as a thin layer on the PES substrate membrane, and the obtained GO/PES membrane was used in the removal of different contaminants from the aqueous solution. As previously explained, the properties of natural PES

combined with GO are thought to make a better composite for color removal and water purification, and Monte Carlo (MC) simulation is necessary to validate the pollutants' adsorption behavior on the surface of the enhanced GO/PES membrane [30]. Moreover, computational techniques can predict the effective behavior of the modified GO by studying the surface interaction types and identifying the optimum MC parameters [31]. A key feature of our work is the combination of experimental results achieved using *in situ* membrane performance evaluation and characterization, complemented by optimization of the results using computational techniques.

## 2. Materials and Methods

### 2.1. Preparation and characterization of GO/PES membrane

GO was synthesized from shredded polyethylene terephthalate (PET) plastic water bottle waste by pyrolyzing them in the presence of a catalyst within a 50 mL enclosed stainless-steel (SS316) autoclave [32 - 34]. In the center of an electric furnace, the reactor was placed, then the furnace was heated to 800°C and held there for an hour. The pyrolysis process happened under autogenic pressure. The system was allowed to cool overnight, and then the resulting material with a yield of 30% was ground into a fine powder.

The resulting GO was supported on a PES membrane (0.20 micron pore size, 47 mm) (Sterlitech, USA) to prevent GO leakage into treated water. The GO/PES coated membrane was prepared according to the following steps, as shown in **Fig.1**. Step 1: Disperse the milled GO into distilled water to give a concentration of 0.1 mg/ml. Step 2: Use a vacuum deposition technique to deposit 10 ml of the GO dispersion onto the PES membrane. Step 3: Allow the GO-coated membranes to dry overnight in a sealed petri dish.

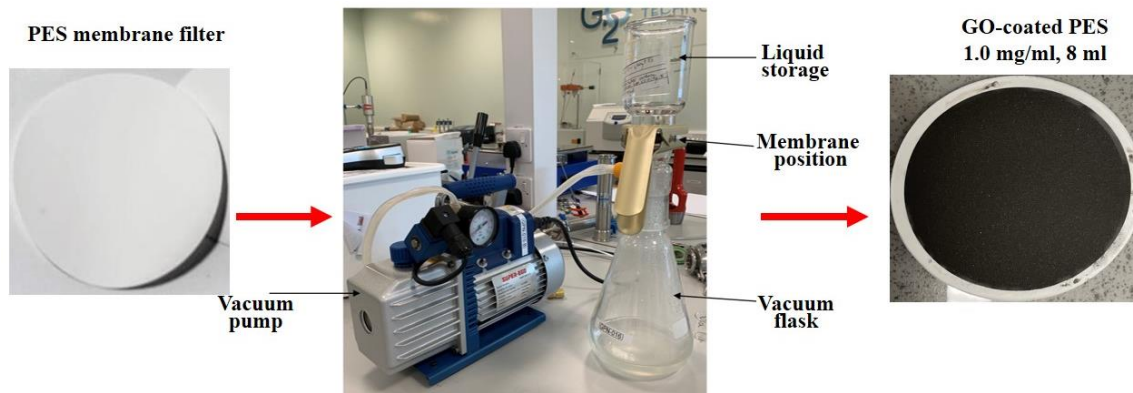


**Figure 1:** Schematic illustration of the steps for preparing GO/PES membranes via vacuum deposition technique.

Some basic characterization of the prepared GO powder and GO/PES membrane was conducted, including surface functional groups analysis using Fourier Transform Infrared (Bruker ALFA FTIR spectrometer) with a range from 400 to 4000  $\text{cm}^{-1}$ , Zeta potential measurement was determined using a Malvern Nanosizer Zeta potential and pH of the suspensions was adjusted using 0.1 M NaOH or HCl. Raman analysis was carried out using spectroscopy (model: SENTERRA Raman spectrometer, Bruker- Germany) and performed using a 514.5 nm laser beam. Transmission Electron Microscope (TEM, TECNAI G20, Netherland) was also used to explore GO morphology while for GO/PES membrane scanning electron microscopy (SEM, JEOL JSM/6360LA, Japan) was used. Surface hydrophilicity using a contact-angle analyzer (Rame-Hart Instrument Co. model 500-FI) with. The Brunauer-Emmett-Teller (BET) surface area and total pore volume were measured using Barret-Joyner-Halenda (BJH) adsorption methods. XPS (a Perkin-Elmer Phi 5300 ESCA system) was used to determine the composition of GO.

## 2.2. Computational study

All of the DFT computations were performed using the Materials Studio Package innovating unit cell generation. Computational optimization of the studied systems used the Perdew–Burke–

Erzerhof exchange–correlation functional (PBE), a projector–augmented wave basis set originated from generalized gradient approximation (GGA) functional, and assuming periodic boundary conditions, and a semi–empirical Grimme's DFT–D3 incorporating van der Waals correction [35, 36]. By using Monte Carlo (MC) simulation, the adsorption of MB dye on the GO/PES membrane was investigated. Adsorption Locator module using current in the charges approach [37] was carried performing MC simulation using Universal force field, and the fundamental MC simulation methods that were applied in this study were laid forth by Frenkel and Smit [30]. In this investigation, the MD simulation was also run. The electrostatic and van der Waals terms were handled in the MD simulations using the Ewald and group-based approaches, respectively.

### *2.3. Performance evaluation and analytical protocols*

Batch experiments were carried out to examine the adsorption efficiency of the GO/PES membrane in a Sterlitech HP4750 dead end filtration cell (**Fig. S1**), operated at 25 °C, transmembrane pressure (TMP) of 0.25 bar with effective membrane surface area of 17.34 cm<sup>2</sup> using methylene blue (MB) dye, Gentimycin sulphate (GMS) antibiotic, and Na<sub>2</sub>SO<sub>4</sub> and MgSO<sub>4</sub> salts in aqueous solution (all chemicals were purchased from Sigma Aldrich and used without further modification). The feed pH was initially lowered by using 0.1M HCL and was raised gradually by adding 0.1M NaOH.

Flux was recorded by measuring the mass of permeate collected over a measured time period using **eq.1**

$$J = V/(A \times \Delta t) \quad (1)$$

where, J is permeate flux (including water and unremoved contaminant transfer through the membrane), A(m<sup>2</sup>) is the membrane area, V(L) is permeate volume and Δt (h) is time the

sampling. The rejection % was recorded by measuring the percentage quantity of contaminant that the membrane is able to remove from water and it was calculated according to **eq.2**:

$$R\% = (1 - C_p/C_f) \times 100 \quad (2)$$

where  $C_f$  and  $C_p$  are the concentrations of contaminant in feed and permeate, respectively.

Similarly, the permeability  $P$ , is the scaling of permeate flux by the filtration pressure, calculated according to **eq. 3**:

$$P = V/(A \times \Delta t \times p) \quad (3)$$

where  $p$  is filtration pressure.

Dye filtration tests were carried out with 100 ml of aqueous MB solution at initial concentration  $10 \text{ mgL}^{-1}$ . The dye was agitated with a magnetic stirrer throughout experiments, to minimize the effects of concentration polarization. The mass of dye permeating through the cell was measured and timed in incremental quantities of 10 mL, Dye absorbance was measured using single frequency UV absorption (Biomate UV) at  $\lambda = 664 \text{ nm}$ . The procedure is iterated until 60 mL has permeated through the cell, after which time the apparatus is depressurized and disconnected.

Analogous procedure to MB filtration the initial Gentamicin Sulphate (GMS),  $\text{Na}_2\text{SO}_4$  and  $\text{MgSO}_4$  concentration is  $10 \text{ mgL}^{-1}$ . The Concentration of single salt solution was conducting by measuring the conductivity of the salt solution using a conductivity meter (Fisher Scientific 09–330 Traceable Bench).

#### *2.4. Optimization of the adsorption process*

To optimize adsorption conditions, we tried to establish a relationship between factors and responses, according to a response surface methodology model. The selected matrix for the response surface methodology followed the Box–Behnken design [38] with 17 trials [39]. To evaluate the adsorption process performance, three factors were used: A (time, min.); B (initial

concentration, mg L<sup>-1</sup>); and C (solution pH), at three levels of -1, 0, and 1 as illustrated in **Table S1, S2, S3**. Data analysis and optimization were carried out using Design-Expert 13 software.

*Leaching test of GO from GO/PES membrane*

### **3. Results and Discussion**

#### *3.1. Characterization of GO and GO/PES membrane*

Raman spectroscopy is a potent tool for analyzing the molecular bonding characteristics of carbon-based materials. The Raman spectra recorded for prepared GO from waste mineral water bottles (**Fig. 2a**) exhibit the two characteristic peaks of graphitic carbon materials, the D-band 1340 cm<sup>-1</sup> and the G-band at 1595 cm<sup>-1</sup>, assigned to defects in the graphene layer and the sp<sup>2</sup> hybridized carbon system, respectively [40]. However, the intensity ratio of the D and G bands ( $I_D/I_G$ ) that quantify the relative levels of disorder is 0.68, which confirms that the obtained GO nanosheets has low structural defects ratio. Furthermore, TEM imaging (**Fig. 2b**) shows the GO nanosheets as irregular agglomerated and individual nanosheets. Meanwhile, the survey XPS spectrum as shown in **Fig. 2c**, demonstrates two main peaks at the binding energy of 533 eV and 285 eV corresponding to the O1s and C1s peaks respectively. It is clearly evident from **Fig. 2c** the obtained GO is not highly oxidized. By curve-fitting analysis (**Fig. 2d**), the C1s spectrum of GO was deconvoluted into four peaks at 284.5, 285.3, 287 and 289.5 eV, corresponding to the sp<sup>2</sup> carbon in aromatic rings, the epoxide, C=O and the carboxyl functional groups, respectively [41, 42]. The dominant C-C/C=C peak at 284.5eV indicating a considerable sp<sup>3</sup>/sp<sup>2</sup> carbon regions in GO structure.

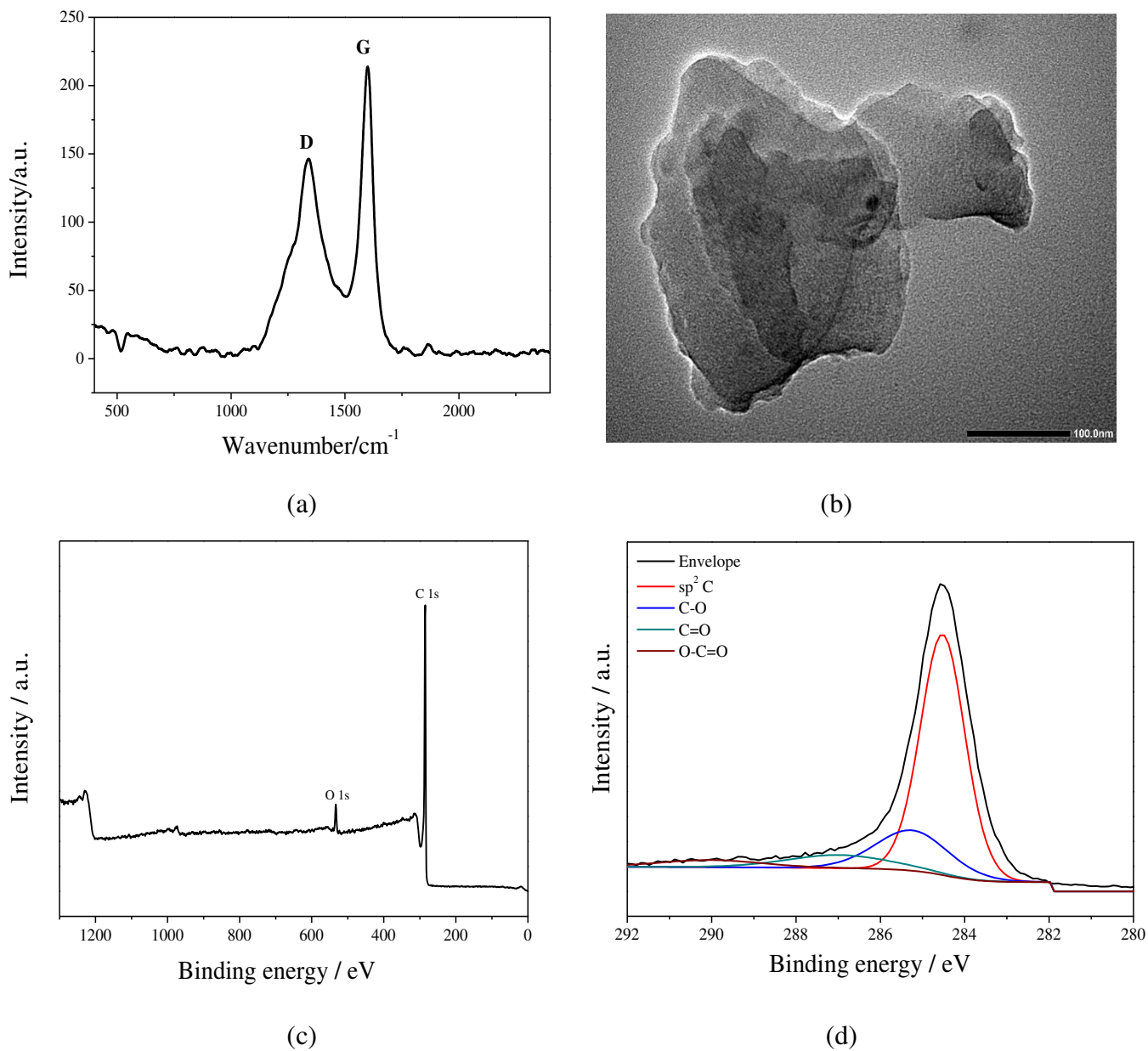
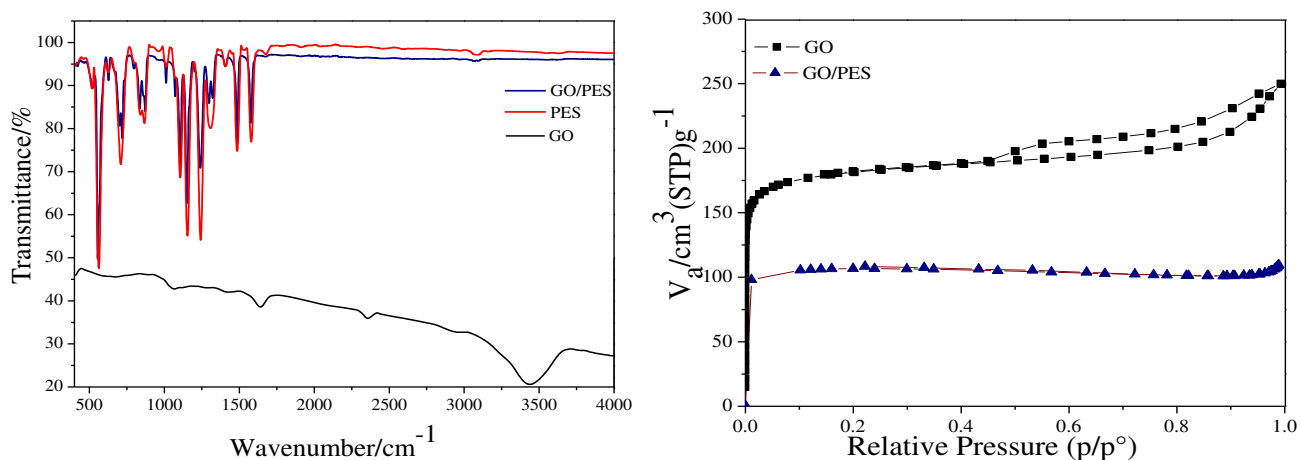


**Figure 2:** (a) Raman spectrum, (b) TEM image, (c) XPS survey spectrum and (d) C1s high-resolution XPS spectra for prepared GO nanosheets.

The functional groups of the prepared GO, PES and GO/PES membrane were investigated using Fourier transform infrared spectroscopy, as shown in **Fig. 3a**. The FTIR spectrum of GO consisted of a strong broad band at 3446 cm<sup>-1</sup>, corresponding to O-H stretching, while the band at

1636  $\text{cm}^{-1}$  can be attributed to the OH stretching and bending vibration of water molecules adsorbed on graphene oxide. However, the bands at 1420, 1272 and 1057  $\text{cm}^{-1}$  corresponded to C-OH, C-O-C and C-O bend respectively reflecting an oxygen content in GO, consequently its adsorption reactivity will be increased [26, 43- 46]. While the characteristic spectrum of the PES membrane included aromatic skeletal bonds between 1400  $\text{cm}^{-1}$  to 1700  $\text{cm}^{-1}$ , and C-O-C stretching bonds at 1200 to 1320  $\text{cm}^{-1}$ . In addition bands observed at about 1350 and 1160  $\text{cm}^{-1}$  were referred to asymmetric and symmetric stretches of sulfone groups ( $\text{SO}_2$ ) in PES. The FTIR spectra of the GO/PES membrane was found to be similar to the PES membrane because there is no chemical bonding of GO to PES substrate, as it is a physical coating process, in addition GO/PES membrane has less signal intensity due to GO layer hinder. The recorded surface area by using BET device of GO and GO/PES membrane were placed in **Fig. 3b**. It is clear that the adsorption-desorption isotherms of  $\text{N}_2$  for GO appears as characteristic IUPAC-type IV nature and exhibits meso- and macroporosity, that could be attributable to the inter-layer spaces between the graphene sheets. The  $\text{N}_2$  sorption isotherms of GO/PES membrane shows narrow hysteresis loop and large specific volume adsorbed at low relative pressures, indicating the presence of meso- and macropores, in addition the hysteresis loop rising above a relative pressure of 0.9 and not reaching saturation, which prevents them from meeting at the endpoint and this phenomenon called "Open hysteresis" [47]. **Table S4** shows the produced specific surface area with main pores diameter and total pore volume for GO and GO/PES membrane. It is worthy to note that the total pore volume and mean pore diameter of GO as powder is higher than those of GO supported on PES membrane. The distribution of the average pore sizes was observed using the BJH method as shown in **Fig.3c** and **Fig. S2a and S2b**, whereas GO and GO/PES membrane showed similar pore size distribution with co-existence of textural meso and macropores which

improves the adsorption process. In addition to the membrane's effective pore size, the charge density of functional groups and the membrane's hydrophilicity have substantial impact on the performance of NF membranes. However, surface potential measurements are a useful method for determining the charge density of the surface functional groups, which dependent on the feed conditions, such as pH. Surface potential of GO/PES membrane measured for a range of pH values is shown in **Fig. S3**. GO/PES membrane have a negative surface potential (-28 mV) at neutral pH because they are decorated with oxygenated groups, which declined to -2 mV at pH 2 due to protonation of oxygenated groups. SEM image in **Fig.3d** shows a dense porous layer of GO on the PES substrate. The stacked GO nanosheets on the membrane surface forming filtering channels for water molecules and pollutant cations [48]. The contact angle between the GO/PES membrane surface and water was used to measure the hydrophilicity of the membrane, and the contact angle was found to be  $56.5^\circ$  as shown in **Fig.3e**. The results of contact angle for GO and GO/PES membrane (**Fig. 3e & f**) are illustrated in **Table S5**. The GO/PES membrane was found to be more hydrophilic than pure PES, suggesting incorporation of GO increases the membrane's hydrophilicity due to the presence of numerous oxygenated functional groups in GO which can attract more water molecules on the surface [49, 50].



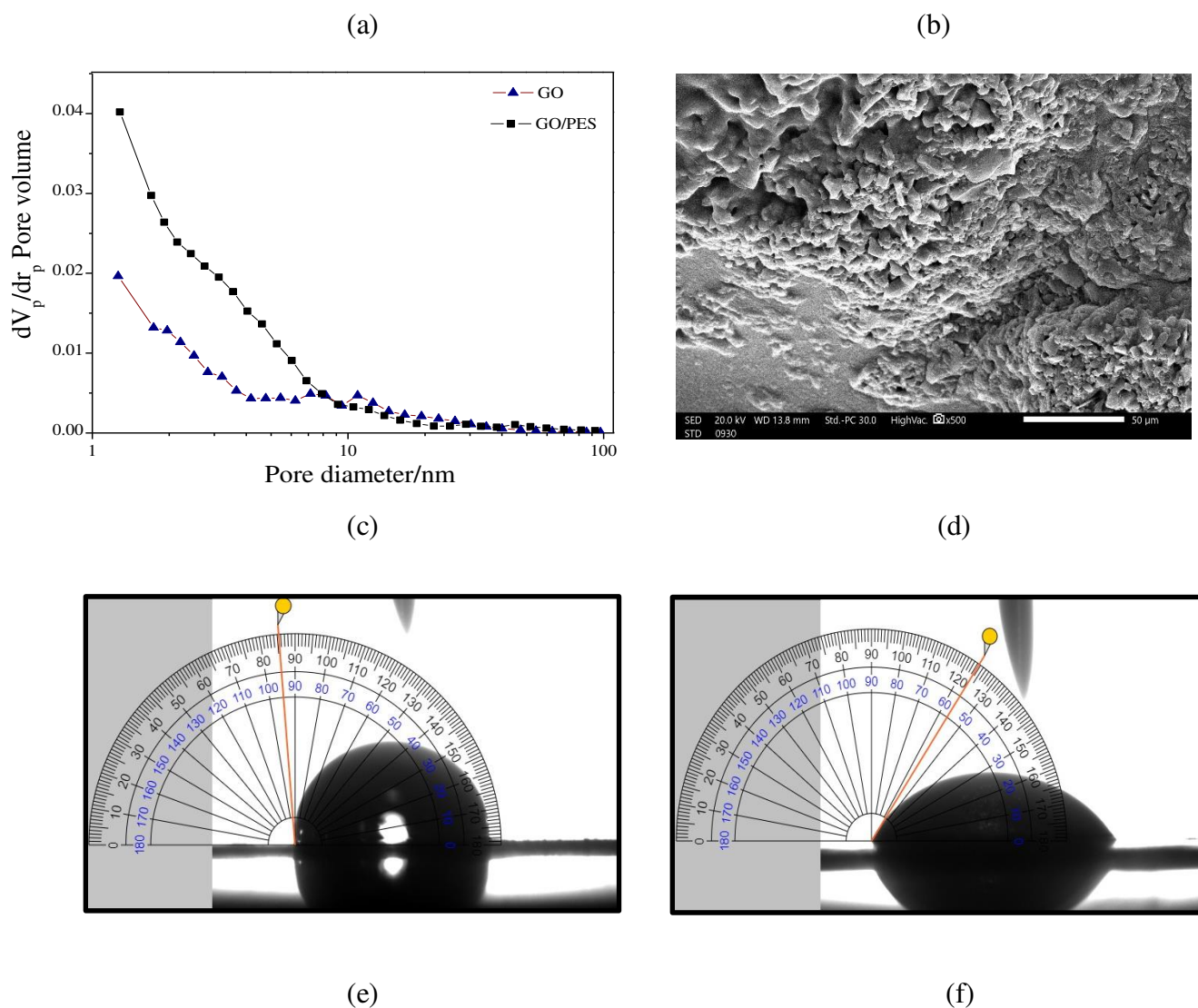
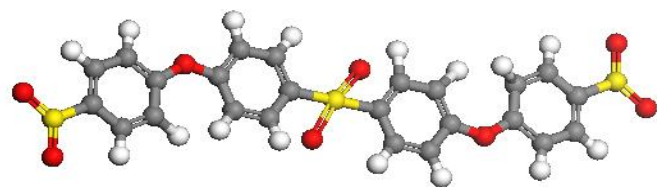
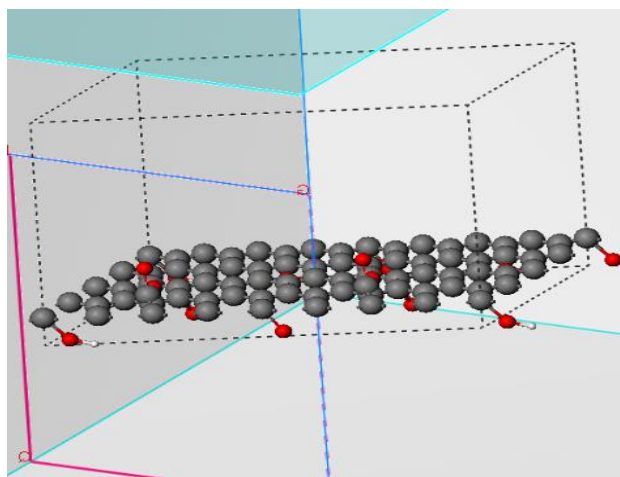


**Figure 3:** (a) FTIR spectra, (b)  $\text{N}_2$  adsorption–desorption isotherms, (c) average diameter distribution, (d) SEM image and contact angle of (e) PES, (f) GO/PES membrane.

### 3.2. Computational Simulation model

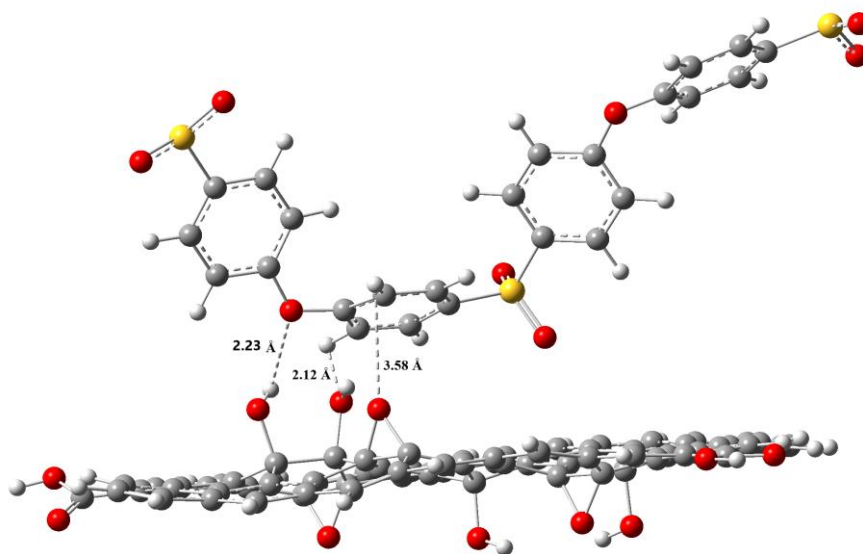
To study the interaction between GO and PES, optimization results were generated and displayed in **Fig.4** as the studied structures processed via DFT postulation. The interaction between the optimized GO and PES was generated with three H-bond formation based on the type of oxygen atoms distributed on the GO layer. As a result, the current work estimated a hydrogen bonds

formation at a distance of 2.17 Å and 2.35 Å between the hydrogen atom of the GO layer and the sulfur atom of the PES membrane (**Fig.4a**) and the other between the different oxygen forms of GO and hydrogen atoms of PES. The distance between the active contact sites of the optimized interaction system can also be used to gauge the degree of interaction. The bond lengths between the GO two oxygen molecules and the hydrogens in PES are 2.12 Å and 3.58 Å, while H-bond present between oxygen of PES and H of GO-OH group has a length of 2.23 Å. (**Fig.S4**).



(a)

(b)



(c)

**Figure 4:** Computational optimization using DFT/GGA/PBE level for (a) GO nanoparticles, (b) PES membrane, and (c) GO/PES interacted structure.

Adsorption Locator calculations deal with the lowest configuration that was produced by the dry adsorption of MB dye as an example for cationic pollutant on the GO/PES nanostructure surface is shown in **Fig. 5**. It was previously reported that MB dye molecule contains many donor and acceptor sites for hydrogen bonding (HBs) [51]. The model construction was developed by adsorption estimation of MB dye molecule onto GO/PES membrane surface. **Fig. 5b** displayed the best adsorption model for GO/PES membrane towards MB dye. To investigate some important non-covalent interactions, it was predicted the formation of H-bond between H atom of MB and epoxy oxygen of combined GO nanostructure with distance of 2.63 Å. Furthermore, the hydrogen atom of MB molecule is linked to the oxygen atom of the combined GO nanosheets at a distance of 2.82 Å. Other additional H-bonds between sulfur atom of MB and H atom of OH group in GO with a distance of 3.06 Å. The combined GO/PES was developed with other locator simulation to include MB molecule and this leading to some interaction modification in the GO/PES system based on the strength of MB adsorption. According to the results of the energetic parameters, the processed model generated the energies of adsorption ( $E_{ads}$ ), contact ( $E_{int.}$ ), and deformation parameter ( $E_{def}$ ) of the studied MB dye on the GO/PES membrane as well as substrate-adsorbate configurations ( $dE_{ads}/dN_i$ ), in which one of the adsorbate components has been removed. The best estimated module possesses  $E_{ads}$  value of -48.72 kcal/mol, leading to adsorption of MB on the GO/PES membrane with negative value and this is a realistic point for energetically advantageous exothermic adsorption and spontaneous with

intermolecular interactions with interaction energy (Eint.) of 34.19 kcal/mol. Other important parameters such Edef and dEads/dNi estimated -14.53 kcal/mol and -48.31 kcal/mol, respectively.

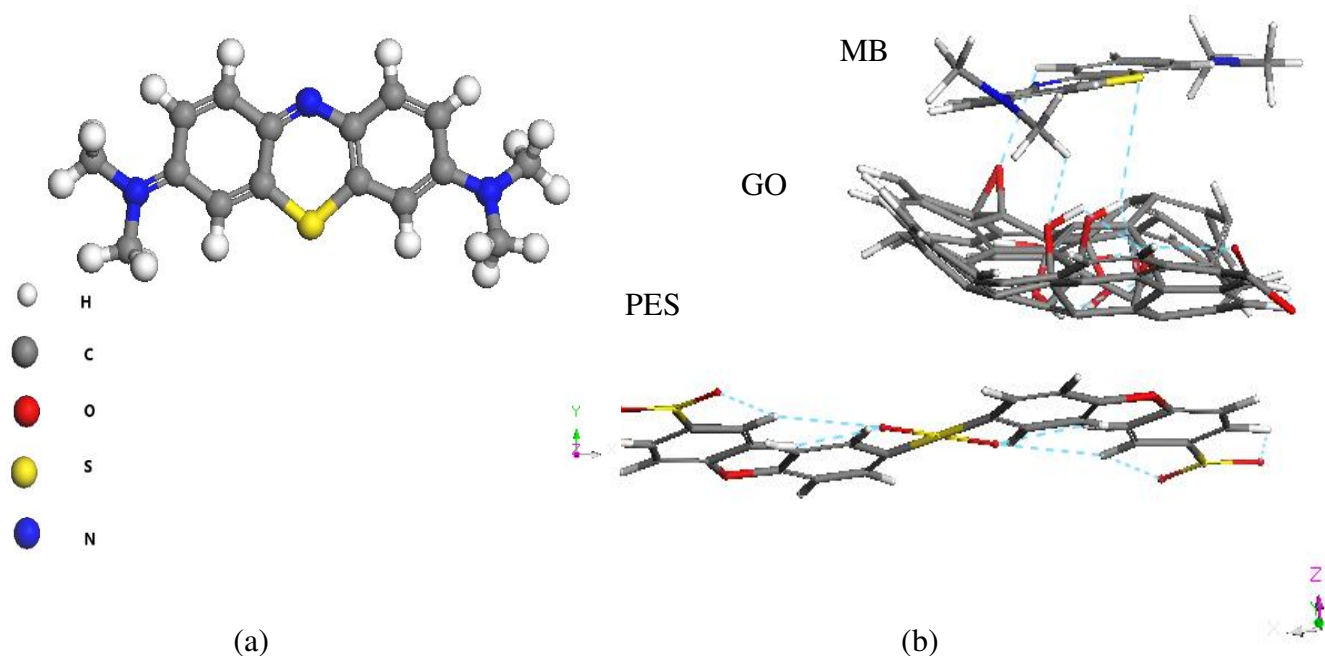


**Figure 5:** (a) computational optimization using DFT/GGA/PBE level for MB molecule, (b) Molecular adsorption modules originated from simulated annealing calculation of GO/PES/MB systems with H-bond distances.

### 3.3. GO/PES membrane performance evaluation

The GO/PES membrane performance was evaluated as shown in **Fig. 6a** by measuring how pure water flux responded to the operating pressure differential across the membrane. It was noticed that, over the examined pressure range up to 2 bars, the membrane showed a proportionate flux increase with the applied pressure gradient. On the other hand, the GO/PES membranes with different GO loadings were tested for water permeability. It was observed that, the amount of

GO loaded on the PES substrate has an inverse correlation with the permeability of the GO/PES membrane as shown in **Fig. 6b**. It is anticipated that the resistance of the GO layers will predominate the overall resistance for flow through the membrane [20, 52] whilst, as more GO is loaded on the PES substrate, the resistance of the GO layer rises linearly because the chemical composition of the deposited GO layer and the alignment of the GO sheets determine which specific resistance it produces [9, 53]. Therefore, to obtain great performance, an ultrathin and aligned layer of GO made up of just a few GO sheets is preferred to be loaded on the underlying substrate, which have some inherent surface roughness, therefore a minimum thickness of GO layer is required to assure defect-free coating of GO. However, the separation performance of the membrane produced by the synthesis of GO layer coatings less than  $18 \text{ mg/m}^2$  was subpar as investigated by Aher et al. [20].

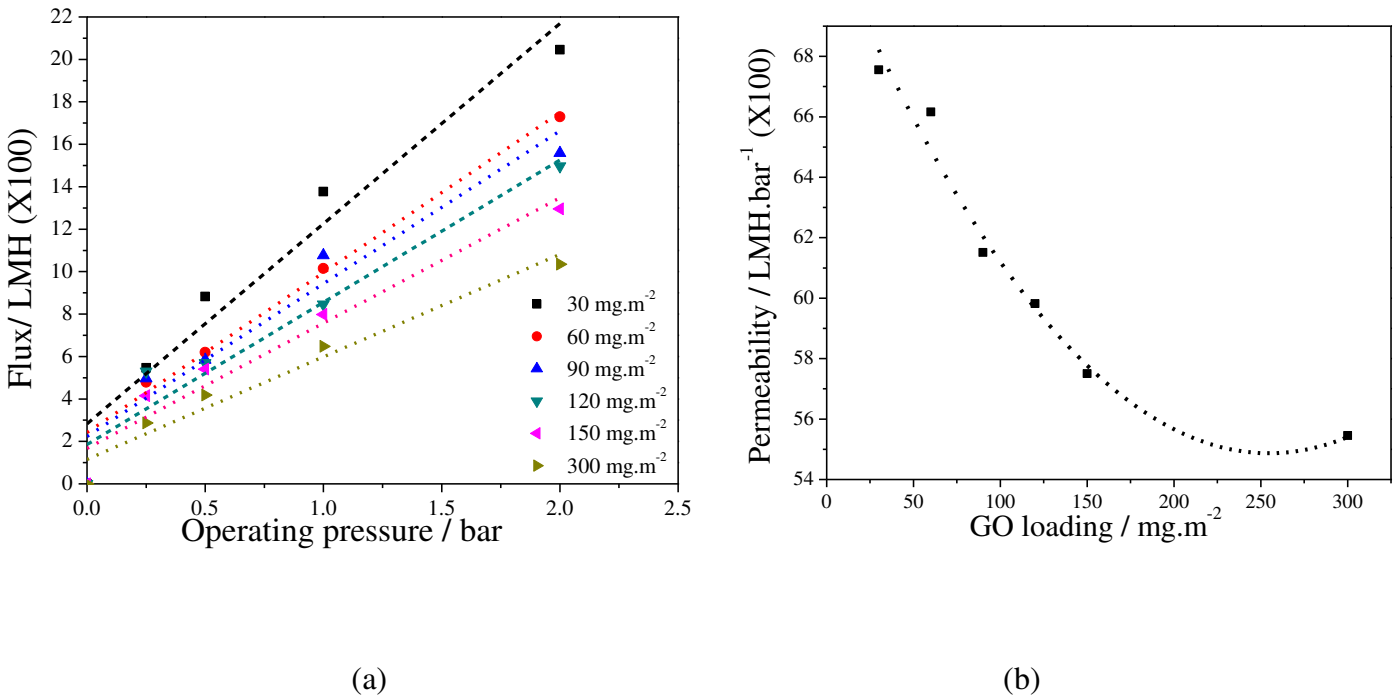


**Figure 6:** (a) Flux-pressure responsiveness and (b) Permeability of GO/PES membrane with different loadings of GO.

The removal of MB and GMS as organic pollutants and Na<sub>2</sub>SO<sub>4</sub> and MgSO<sub>4</sub> as single salt was investigated to evaluate the separation performance of GO/PES membrane under 0.25 bar. As shown in **Fig. 7 a, b**, the rejections of the membrane to the examined pollutants follow the order of GMS > MB > Na<sub>2</sub>SO<sub>4</sub> > MgSO<sub>4</sub>. The rejection % of GMS and MB can reach 93% and 91%, respectively, while the rejection % of Na<sub>2</sub>SO<sub>4</sub> and MgSO<sub>4</sub> reached 67% and 64%, respectively. The separation of MB and GMS depend mainly on the electrostatic adsorption interaction between cationic MB and GMS, and the negative charge surface of GO/PES membrane [54, 55]. In addition, the relative molecular weight of the organic molecule has an additional effect, whereas the larger the relative molecular weight (Mwt. of GMS is 463 g mol<sup>-1</sup>, Mwt. of MB is 319.83 g mol<sup>-1</sup>) the more sieving hindrance of the membrane, and the greater rejection rate [56]. However, the development of molecular sieves based on graphene will open the door in the future to extremely selective separations. On the other hand, Mg<sup>2+</sup> rejection depends on Donnan exclusion in addition to ionic sieving [57] and Na<sup>1+</sup> rejection depends on steric hindrance since it has weak electrostatic repulsion and that results were found to be consistent with literature [7, 58 - 60].

Generally the fabricated GO/PES membrane has a high porosity, hydrophilicity and negative charged surface due to the deprotonation of the carboxyl and hydroxyl group in GO and the sulfonic group in PES, therefore it exhibits better rejection performance to high molecular weight positive charged organic pollutants as GMS and MB in addition to Na<sub>2</sub>SO<sub>4</sub> and MgSO<sub>4</sub> even though both salts consist of SO<sub>4</sub><sup>2-</sup> ions, a schematic suggestion of all interaction mechanisms of GO/PES membrane NF was shown in **Fig. 7c**.

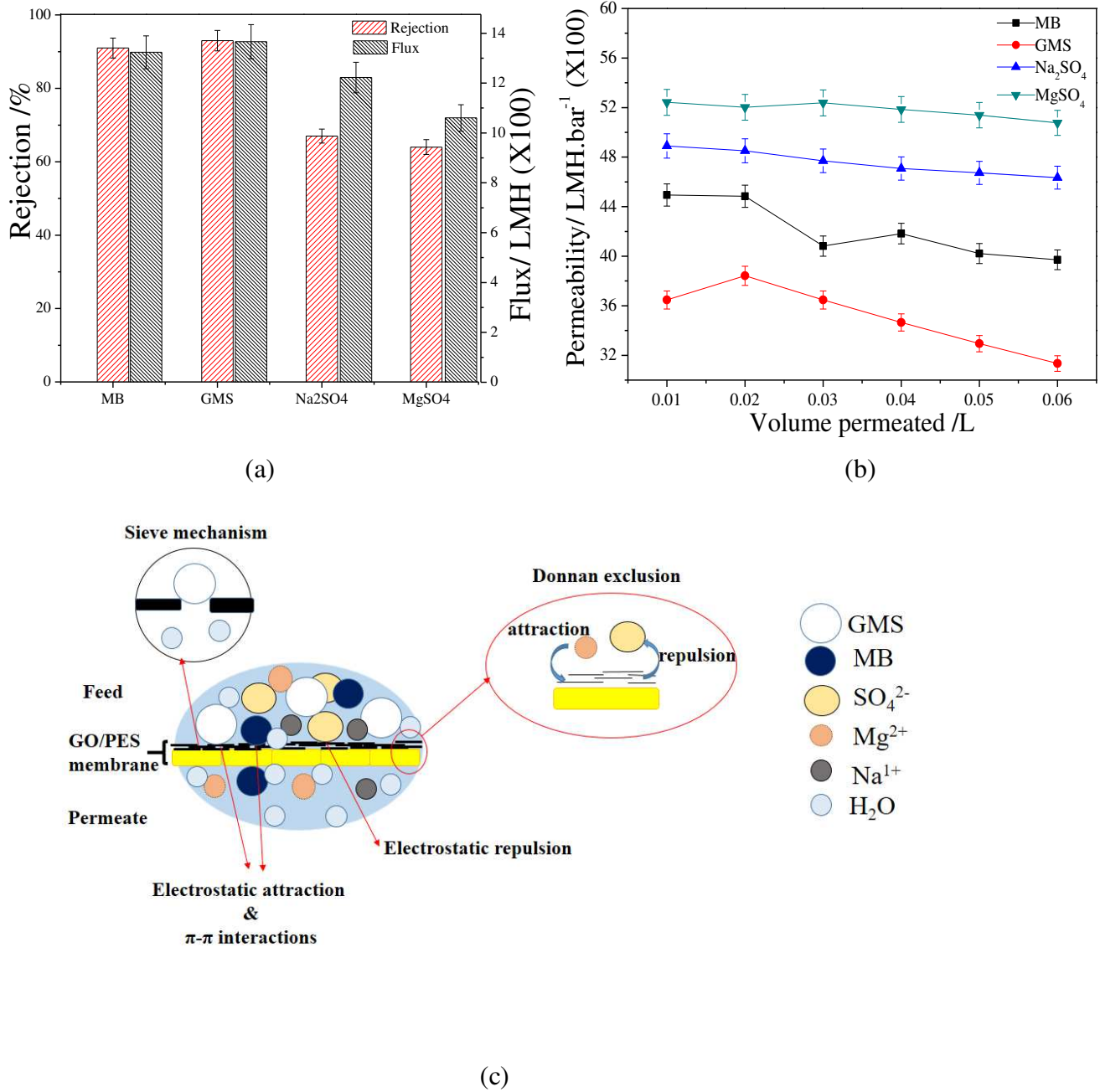


**Figure 7:** (a) rejection % and permeate flux, and (b) permeability through GO/PES membrane with GO loading 60 mg.m<sup>-2</sup> at 25°C and pH 7, (c) a schematic illustration of all interaction mechanisms of GO/PES membrane NF.

### 3.4. Optimization of membrane performance

Batch filtration studies with time range 0-3 min., initial contaminant concentrations of 5, 10, 15 mg L<sup>-1</sup> for MB, GMS, Na<sub>2</sub>SO<sub>4</sub> and MgSO<sub>4</sub>, and solutions pH ranged between 2 to 12 were conducted to find the optimum conditions for the filtration process. The effects of time, initial contaminant concentration at various solution pH on rejection efficiency are summarized in 3D surface plots as shown in **Fig. 8 and Fig. 9**. In general it was found that the rejection efficiency decreased with increasing initial contaminant concentration, whilst it increased with filtration time. Our observations suggest that, at the start of the experiment, contaminants were adsorbed externally and the adsorption rate increased rapidly. Once the external surface became saturated, the adsorption process occurred through the membrane pores and finally reached a constant value where no more adsorption occurred [61]. Moreover, based on the perturbation plots (**Fig.8g&h, Fig.9g&h**), it was observed that, the solution pH had a significant effect on the filtration performance and its effect is greater than time or initial contaminant concentration effect. The effect of pH on contaminant rejection can be explained by changes in membrane charge and electrostatic attraction/repulsion between ions and membrane [62]. For GMS, the pH of the solution varied from 3 to 9 and it was observed that the rejection % increased with solution pH increasing till it reached pH 8, then decreased with solution pH increasing. That can be explained by, GMS has amphoteric characteristics and usually appears in three different forms: in the cation form at low pH, in the zwitterion form at pH values between 6.1 and 8.7, and in the anion form at high pH as shown in **Fig. S5a**. However, at solution pH values increases from acidic to basic, the zeta potential of GO/PES membrane surface become more and more negatively charged and the rejection % increases until reached pH 8. It was proposed that GMS filtration through GO/PES membrane was dependent on two factors, first, surface charge and functional surface groups, while the second factor is the size of pollutant molecules and

membrane pores size (sieving mechanism). While for MB dye under acidic pH, lower dye rejection % were observed and in neutral and basic pH, the higher dye rejection % were obtained. However, the lower rejection % of MB dye under acidic pH can be attributed to the protonation GO/PES membrane surface and surrounded by many hydronium ions, which compete with MB molecules and that induced the electrostatic repulsion between MB dye and the membrane surface. Conversely, the higher MB dye removal in basic pH can be attributed to the deprotonation of numerous COOH groups of GO into negatively charged COO<sup>-</sup> enhancing the electrostatic attraction between MB molecules and the membrane surface and that was confirmed from the FTIR spectra of the GO/PES membrane before and after MB dye filtration as shown in **Fig. S6**. Whereas, the FTIR spectrum for GO/PES membrane before filtration process was found to be similar to that of GO/PES membrane after filtration process with less signal intensity due to MB layer hinder. Therefore, it is reasonable to anticipate that positively charged molecules will experience "charge concentration polarization" as a result of electrostatic attraction [63, 64]. It is likely to conclude that the higher rejection rates were mainly caused by the increased negative charge on the membrane surface. For Na<sub>2</sub>SO<sub>4</sub> and MgSO<sub>4</sub> by increasing the solution pH, the rejection efficiency first increased until reaching pH 7 and then decreased. The protonation of GO/PES membrane surface in acidic aqueous solution occurred, resulting in affinity interaction between SO<sub>4</sub><sup>2-</sup> and the positively charged membrane surface, which may benefit the passage of SO<sub>4</sub><sup>2-</sup> through the membrane and hinder the passage of Na<sup>+</sup> and Mg<sup>2+</sup>. On the other hand, as proved by zeta potential data, at high pH values the membrane's negative surface charge increased, the water flux of the membrane will be decreased and the salt concentration will be raised indirectly in the permeate; consequently, that may be a factor in the relatively low salt rejection [65 - 67].

The following equations provide the best fit for the quadratic model, which described the statistical relationship between the chosen variables (A: time, B: initial contaminant concentrations, and C: solutions pH) and the response (Rejection) in terms of coded components.

$$\text{Rejection } \%_{GMS} = 82 + 6.5A + 1.38B + 29.38C - 2.25AB + 0.25AC - 3.5BC - 1.00A^2 + 1.25B^2 - 25.75C^2 \quad (4)$$

$$\text{Rejection } \%_{MB} = 53 + 5.13A - 1.00B + 23.88C - 0.75AB + 2.5AC - 6.25BC - 5.5A^2 - 4.25B^2 + 8.5C^2 \quad (5)$$

$$\text{Rejection } \%_{Na_2SO_4} = 59 + 5.87A - 1.37B - 1.75C - 10AB + 1.75AC + 3.75BC - 7.25A^2 - 5.25B^2 - 37C^2 \quad (6)$$

$$\text{Rejection } \%_{MgSO_4} = 54 + 7.137A + 1B - 2.12C - 1.25AB + 0.5AC + 2.25BC - 1A^2 - 1.25B^2 - 41.5C^2 \quad (7)$$

A positive-sign coefficient indicates a synergistic effect of the element, conversely a negative sign denotes the factor's antagonistic effect [68]. The ANOVA analysis of variance, as shown in **Table S7, S9, S11 and S13** of model validations demonstrated that, the coefficient of determination  $R^2$ , adjusted  $R^2$ , and predicted  $R^2$  which are indices of the quality of the regression are in reasonable agreement whereas the difference is less than 0.2 for GMS, MB and  $Na_2SO_4$ . While for  $Mg_2SO_4$  the difference is more than 0.2 and this may indicate a large block effect. Nonetheless, the coefficient of determination provides many measures of the model's quality, indicating strong agreement between the fitted model's anticipated values and experimental results. Since there is a strong correlation between the expected removal rate from the model and the data, therefore it can be conclude that the mathematical model is acceptable and sufficient [68, 69].

In this respect, optimal levels were obtained from the maximum point of the polynomial model to achieve 95.2% rejection % for GMS were 2.4 min filtration time, 5.3 mg  $L^{-1}$  initial concentration at solution pH 8. For MB the rejection % was 91% at filtration time 3 min, initial concentration of 5.8 mg  $L^{-1}$  and 12 of solution pH. For  $Na_2SO_4$  the rejection % was 63.8% at filtration time 3 min, initial concentration of 5 mg  $L^{-1}$  and 7 of solution pH, while for  $MgSO_4$  the rejection % was 62% at filtration time 3 min, initial concentration of 9.4 mg  $L^{-1}$  and 7 of solution

pH. Therefore, these results emphasize the necessity and value of using the response surface method to design the experiments which can be considered as an effective choice in the optimization of process parameters [70].

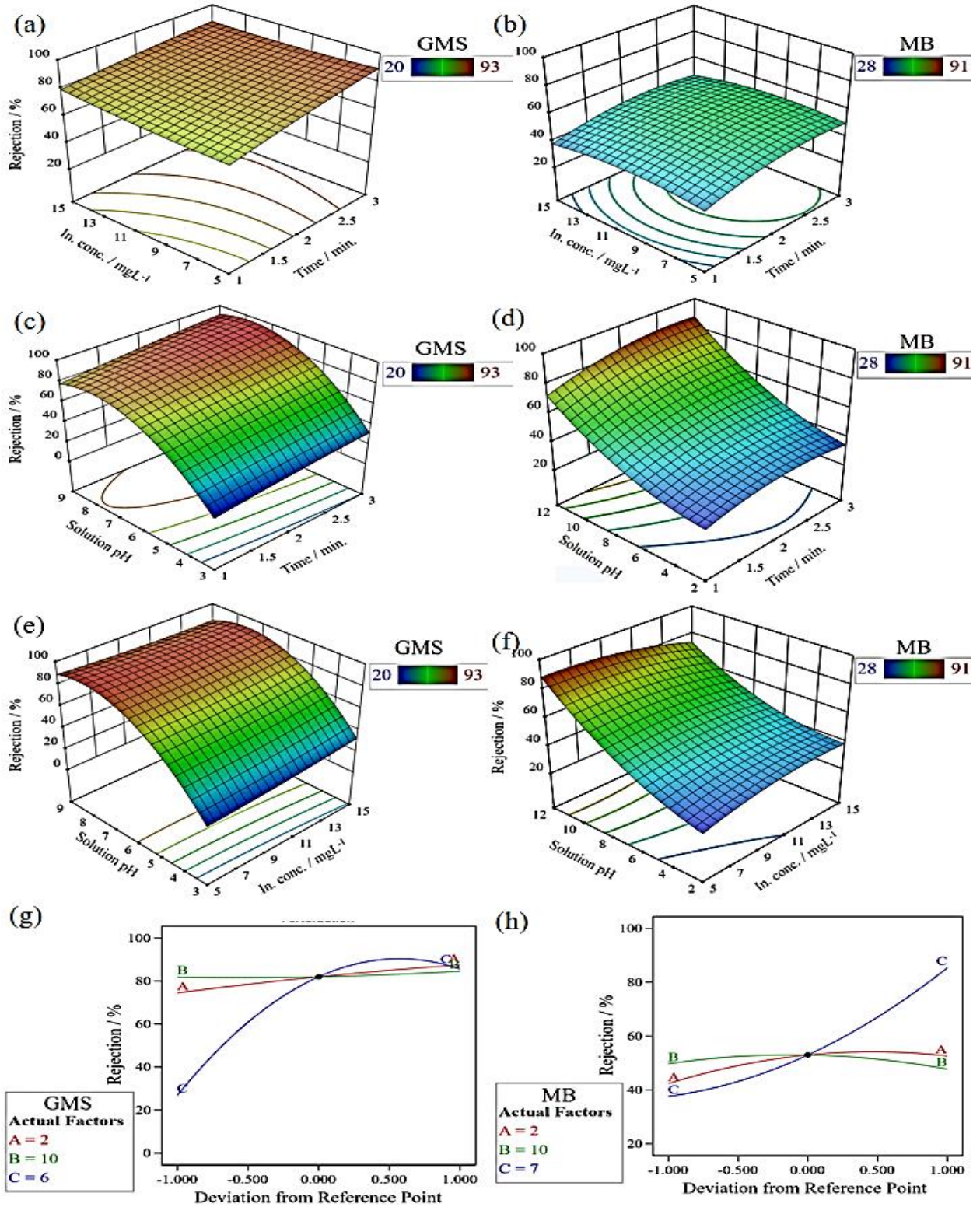


**Figure 8:** 3D plots of GMS and MB rejection % versus filtration process variables through GO/PES membrane.

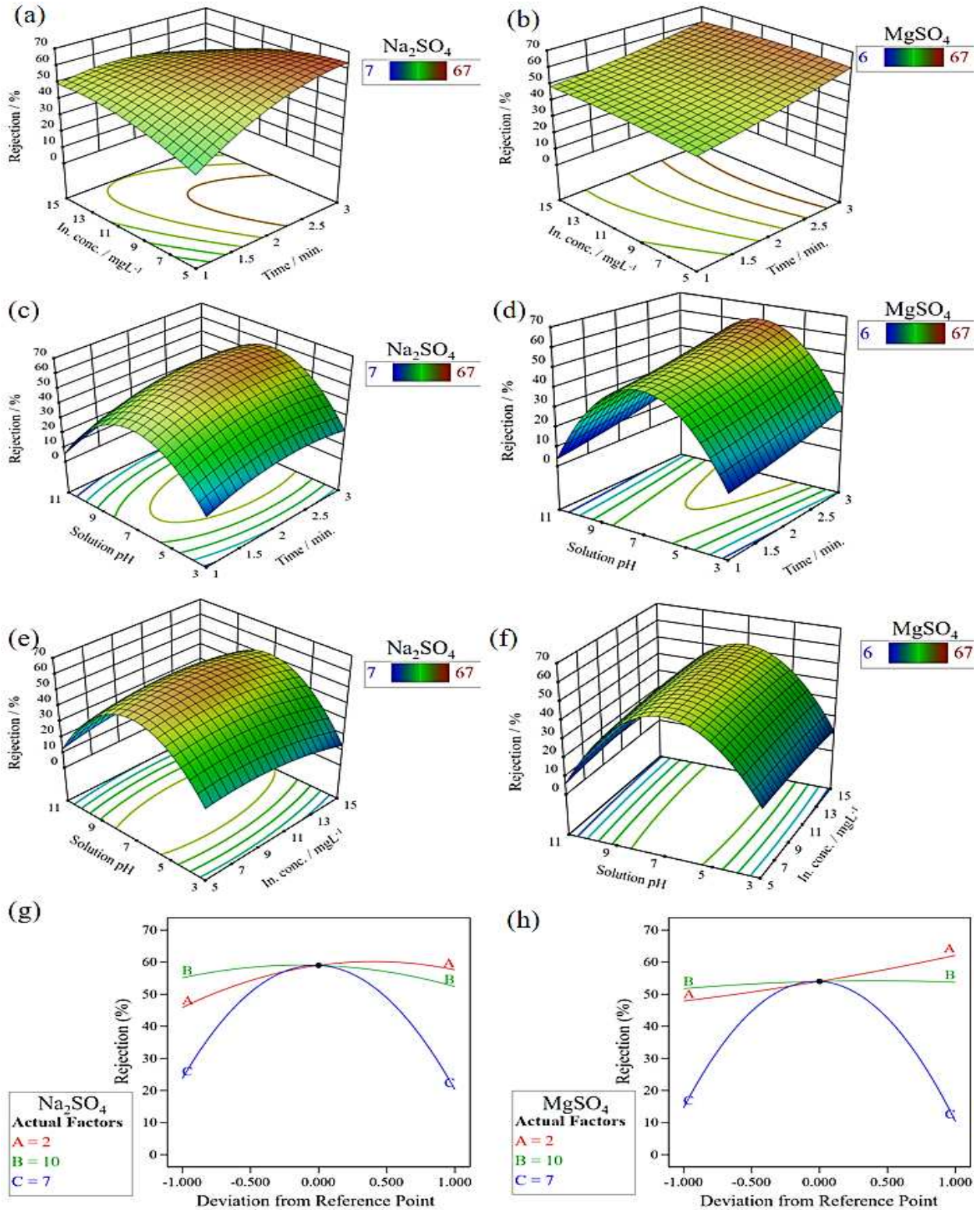


**Figure 9:** 3D plots of  $\text{Na}_2\text{SO}_4$  and  $\text{MgSO}_4$  rejection % versus filtration process variables through GO/PES membrane.

### 3.5. Leaching test of GO from GO/PES membrane

Leaching experiments were conducted to investigate the stability of GO nanosheets bonded to PES membrane with surface area  $17.34 \text{ cm}^2$ , whereas leaching was ascribed to the unreacted GO nanosheets that was physically adsorbed on the PES membrane surface. The initial concentration of GO on the membrane surface was  $60 \text{ mg.m}^{-2}$ . It was found that after 5 days leaching study, 3 mg of GO was leached out of the PES membrane surface by first day with the majority of the leaching about 76%. As shown in **Fig. 10**, the leaching of the GO nanosheets was significant, as approximately 62% of the GO nanosheets remained covalently attached to PES membrane after 5 days.

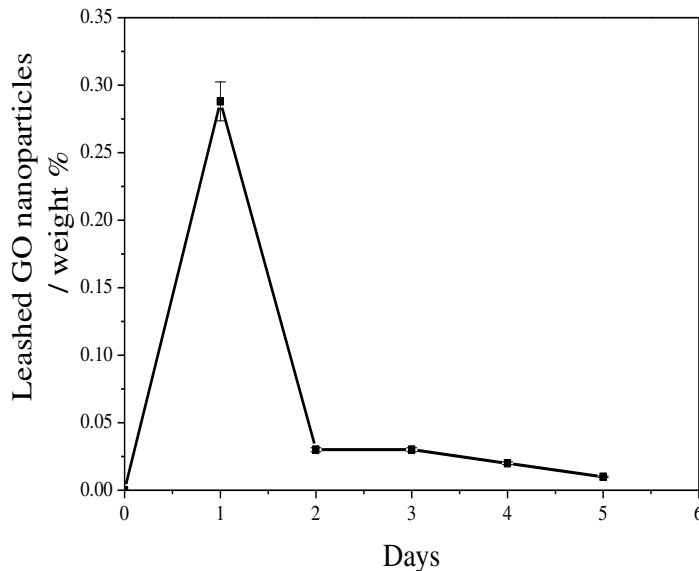


**Figure 10:** The weight % of GO nanosheets leached during 5 days.

It came to light that our environmentally friendly fabricated membrane for NF is practical to use to remove different contaminants from water compared to previous studies, as illustrated in **Table 1**. However, the prepared GO can compete with other carbon-based materials, which can solve one of the environmental sustainability problems by reducing plastic waste pollution. It

was prepared by using a simple one-pot and an easy operational procedure that can easily be scaled up, offering great future potential for industrial production. Furthermore, as the subsequent experiment has demonstrated, carbon based materials may be readily supported on membrane by high vacuum filtering to produce stable membrane that can be used repeatedly at low pressure.

**Table 1:** A comparison of the effectiveness of several carbon/polymer NF membranes used to remove various contaminants

Membrane	contaminant	Rejection (%)	Reference
GO/molybdenum disulphide (MoS <sub>2</sub> )-PVA composite membranes	Na <sup>+</sup>	89	[71]
Polyethersulfone support with polyethyleneimine active layer, doused GO with trimesoyl chloride	Mg <sup>+2</sup>	95.14	[72]
Poly Vinylidene Fluoride (PVDF)/Graphene Oxide (PGO) composite membrane	MO dye,	< 50	[54]
	MB dye	98	
Polyethersulfone support GO/cyclodextrin	Congo red	97	[73]
	Eriochrome	99	
	black T		
GO supported on PES membrane	MB dye	91	This work
	GMS	> 93	
	antibiotics	67	
	Na <sup>+</sup>	64	
	Mg <sup>+2</sup>		

#### **4. Conclusions**

GO was prepared using waste mineral water bottles. The resulting GO was supported on PES membranes and used to remove MB dye, GMS antibiotic, and  $\text{Na}_2\text{SO}_4$  and  $\text{MgSO}_4$  salts from an aqueous solution. The results show that time, solution pH, and contaminant concentration were significant operating parameters affecting membrane performance. The rejections of the membrane towards the examined pollutants follow the order of  $\text{GMS} > \text{MB} > \text{Na}_2\text{SO}_4 > \text{MgSO}_4$ . The performance of the filtration process using the GO/PES membrane mainly depends upon electrostatic attraction/repulsion force and non-covalent interactions between surface membrane charge and contaminants ions, as confirmed by applying DFT, which predicted a best adsorption locator MB model with significant energetic behavior (-48.72 kcal/mol). The prepared GO/PES membranes exhibited acceptable properties as NF membranes for investigated water contaminants and thus could offer a solution to waste disposal and industrial wastewater treatment.

#### **Acknowledgements**

The authors acknowledge the support from The Science, Technology & Innovation Funding Authority (STDF), Grant (Egypt-UK Cooperation: Newton-Mosharafa Program: Leaders in Innovation Fellowships (LIF)) Phase I, Call 7, project No. 44084.

#### **Conflicts of Interest**

The authors declare no conflict of interest.

#### **Authorship contribution statement**

Noha A. Elessawy: Conceptualization, Methodology, Investigation and Writing/original draft.  
James Exley: Methodology, Investigation and editing original draft. Doaa S. El-Sayed: Software, formal analysis. Arafat Toghan & Mohamed Elzokm: Investigation and Writing/original draft.

Sami A. Al-Hussain: Methodology, Writing/review and editing. Abdelaziz H. Konsowa: Conceptualization, Supervision and Validation. Martin Tillotson: Project administration, Writing/review and editing.

## References

1. X. Feng, D. Peng, J. Zhu, Y. Wang, Y. Zhang, Recent advances of loose nanofiltration membranes for dye/salt separation, *Separation and Purification Technology*. 285 (2022) 120228. <https://doi.org/10.1016/j.seppur.2021.120228>
2. C. Vargas-Figueroa, L. Pino-Soto, A. Beratto-Ramos, Y. Tapiero, B.L. Rivas, M.E. Berrio, M.F. Melendrez, R.M. Bórquez, In-situ modification of nanofiltration membranes using carbon nanotubes for water treatment, *Membranes* 13(2023) 616. <https://doi.org/10.3390/membranes13070616>
3. H.B. Lin, J.G. Zhao, N. Lu, Q. Han, J. Wang, J. Guan, X. Wang, F. Liu, Prussian blue/cellulose acetate thin film composite nanofiltration membrane for molecular sieving and catalytic fouling resistance, *Chin J Polym Sci* 41(2023) 593–604. <https://doi.org/10.1007/s10118-023-2950-2>
4. M. Batool, M. Abbas, I. Khan, M. Khan, M. Saleem, A. Khan, K. Deen, M. Batool, A. Khan, S. Zhu, N. Ahmad, Response surface methodology modeling correlation of polymer composite carbon nanotubes/chitosan nanofiltration membranes for water desalination, *ACS ES&T Water* 3 (202) 1406-1421. <https://doi.org/10.1021/acsestwater.3c00107>
5. R. Dai, H. Zhou, T. Wang, Z. Qiu, L. Long, S. Lin, C.Y. Tang, Z. Wang, Nanovehicle-assisted monomer shuttling enables highly permeable and selective nanofiltration membranes for water purification, *Nat Water* 1(2023) 281–290. <https://doi.org/10.1038/s44221-022-00010-3>

6. P. Li, H. Xie, Y. Bi, C. Miao, K. Chen, T. Xie, S. Zhao, H. Sun, X. Yang, Y. Hou, Q. Niu, Preparation of high flux organic solvent nanofiltration membrane based on polyimide/Noria composite ultrafiltration membrane, *Applied Surface Science* 618(2023)156650.  
<https://doi.org/10.1016/j.apsusc.2023.156650>
7. X. Geng, J. Wang, Y. Ding, W. Zhang, Y. Wang, F. Liu, Poly(vinyl alcohol)/polydopamine hybrid nanofiltration membrane fabricated through aqueous electrospinning with excellent antifouling and chlorine resistance, *Journal of Membrane Science* 632 (2021) 119385.  
<https://doi.org/10.1016/j.memsci.2021.119385>
8. R. Mohamat, S.A. Bakar, A. Mohamed, M. Muqoyyanah, M.H.D. Othman, M.H. Mamat, M.F. Malek, M.K. Ahmad, Y. Yulkifli, S. Ramakrishna, Incorporation of graphene oxide/titanium dioxide with different polymer materials and its effects on methylene blue dye rejection and antifouling ability, *Environ Sci Pollut Res* 30(2023)72446–72462.  
<https://doi.org/10.1007/s11356-023-27207-7>
9. Y. Liu, S. Zheng, P. Gu, A. Ng, M. Wang, Y. Wei, J. Urban, B. Mi, Graphene-polyelectrolyte multilayer membranes with tunable structure and internal charge, *Carbon* 160 (2020) 219-227. <https://doi.org/10.1016/j.carbon.2019.12.092>
10. H. Mahdavi, N. Zeinalipour, M. Kerachian, A. Heidari, Preparation of high-performance PVDF mixed matrix membranes incorporated with PVDF-g-PMMA copolymer and GO@SiO<sub>2</sub> nanoparticles for dye rejection applications, *Journal of Water Process Engineering* 46 (2022) 102560. <https://doi.org/10.1016/j.jwpe.2022.102560>
11. P. Balkanloo, M. Mahmoudian, M. Hosseinzadeh, A comparative study between MMT-Fe<sub>3</sub>O<sub>4</sub>/PES, MMT-HBE/PES, and MMT-acid activated/PES mixed matrix membranes, *Chem Eng J* 396(2020)125188. <https://doi.org/10.1016/j.cej.2020.125188>

12. O, Mahlangu, G. Mamba, B.Mamba, A facile synthesis approach for GO-ZnO/PES ultrafiltration mixed matrix photocatalytic membranes for dye removal in water: Leveraging the synergy between photocatalysis and membrane filtration, *Journal of Environmental Chemical Engineering* 11 (2023) 110065. <https://doi.org/10.1016/j.jece.2023.110065>
13. S. Dadari, M. Rahimi, S. Zinadini, Novel antibacterial and antifouling PES nanofiltration membrane incorporated with green synthesized nickel-bentonite nanoparticles for heavy metal ions removal, *Chemical Engineering Journal* 431 (2022) 134116. <https://doi.org/10.1016/j.ccej.2021.134116>
14. G. Moradi, S. Zinadini, L. Rajabi, Development of the tetrathioterephthalate filler incorporated PES nanofiltration membrane with efficient heavy metal ions rejection and superior antifouling properties, *Journal of Environmental Chemical Engineering* 8 (2020) 104431. <https://doi.org/10.1016/j.jece.2020.104431>
15. M. Sharma, P. Alves, L. Ferreira, Effect of activated carbon nanoparticles on the performance of PES nanofiltration membranes to separate kraft lignin from black liquor, *Journal of Water Process Engineering* 52 (2023) 103487. <https://doi.org/10.1016/j.jwpe.2023.103487>
16. J.M. Exley, T.N. Hunter, T. Pugh, M.R. Tillotson, Influence of flake size and electrolyte conditions on graphene oxide adsorption of ionic dyes, *Powder Technology* 421 (2023) 118387. <https://doi.org/10.1016/j.powtec.2023.118387>
17. M. Fouladi, M K. Heidari, O. Tavakoli, Performance comparison of thin-film nanocomposite polyamide nanofiltration membranes for heavy metal/salt wastewater treatment, *J Nanopart Res* 25(2023) 77. <https://doi.org/10.1007/s11051-023-05727-0>

18. F. Gholami, G. Ghanizadeh, A.A. Zinatizadeh, S. Zinadini, H. Masoumbeigi, Design of a new polyethersulfone nanofiltration membrane with anti-fouling properties using supported protic ionic liquid modification for dye/salt removal, *Water Environment Research*, 95(2023), e10829. <https://doi.org/10.1002/wer.10829>
19. M. El Achaby, F.Z. Arrakhiz, S. Vaudreuil, E.M. Essassi, A. Qaiss, Piezoelectric  $\beta$ -polymorph formation and properties enhancement in graphene oxide – PVDF nanocomposite films, *Appl. Surf. Sci.* 258 (2012), 7668–7677. <https://doi.org/10.1016/j.apsusc.2012.04.118>.
20. A. Aher, T. Nickerson, C. Jordan, F. Thorpe, E. Hatakeyama, L. Ormsbee, M. Majumder, D. Bhattacharyya, Ion and organic transport in Graphene oxide membranes: model development to difficult water remediation applications, *J. Membr. Sci.*, 604 (2020), 118024. <https://doi.org/10.1016/j.memsci.2020.118024>
21. S. Zinadini, A. Zinatizadeh, M. Rahimi, V. Vatanpour, H. Zangeneh, Preparation of a novel antifouling mixed matrix PES membrane by embedding graphene oxide nanoplates, *Journal of Membrane Science* 453(2014)292–301. <https://doi.org/10.1016/j.memsci.2013.10.070>
22. N. Li, W. Wang, C. Ma, L., Zhu, X. Chen, B. Zhang, C. Zhong, A novel conductive rGO/ZnO/PSF membrane with superior water flux for electrocatalytic degradation of organic pollutants, *J. Membr. Sci.* 641 (2022), 119901. <https://doi.org/10.1016/j.memsci.2021.119901>.
23. W.S. Hummers Jr., R.E. Offeman, Preparation of graphitic oxide, *J. Am. Chem. Soc.* 80(1958)1339. <https://doi.org/10.1021/ja01539a017>.
24. M. Khansanami, A. Esfandiari, High flux and complete dyes removal from water by reduced graphene oxide laminate on Poly Vinylidene Fluoride/graphene oxide membranes, *Environmental Research* 201 (2021) 111576. <https://doi.org/10.1016/j.jmrt.2022.04.104>.

25. A. Jiříčková, O. Jankovský, Z. Sofer, D. Sedmidubský, Synthesis and applications of graphene oxide. *materials* (Basel). 15(2022) 920. <https://doi.org/10.3390/ma15030920>.
26. D.X. Luong, K.V. Bets, W.A. Algozeeb, M.G. Stanford, C. Kittrell, W. Chen, R.V. Salvatierra, M. Ren, E.A. McHugh, P.A., Advincula, Z. Wang, M. Bhatt, H. Guo, V. Mancevski, R. Shahsavari, B.I. Yakobson, L.M. Tour, Gram-scale bottom-up flash graphene synthesis. *Nature* 577(2020) 647–651. <https://doi.org/10.1038/s41586-020-1938-0>
27. K.M. Wyss, J.L. Beckham, W. Chen, D.X. Luong, P. Hundi, S. Raghuraman, R. Shahsavari, J.M. Tour, Converting plastic waste pyrolysis ash into flash graphene, *Carbon*. 174 (2021) 430-438. <https://doi.org/10.1016/j.carbon.2020.12.063>
28. W.A. Algozeeb, P.E. Savas, D.X. Luong, W. Chen, C. Kittrell, M. Bhat, R. Shahsavari, J.M. Tour, Flash graphene from plastic waste, *ACS Nano*. 14 (2020)15595-15604. <https://doi.org/10.1021/acsnano.0c06328>
29. P.A. Advincula, D.X. Luong, W. Chen, S. Raghuraman, R. Shahsavari, J.M. Tour, Flash graphene from rubber waste, *Carbon*. 178 (2021) 649-656. <https://doi.org/10.1016/j.carbon.2021.03.020>
30. F. Mohamed, M. Shaban, S.K. Zaki, M.S. Abd-Elsamie, R. Sayed, M. Zayed, N. Khalid, S. Saad, S. Omar, A.M. Ahmed, A. Gerges, H.R. Abd El-Mageed, N.K.Soliman, Activated carbon derived from sugarcane and modified with natural zeolite for efficient adsorption of methylene blue dye: experimentally and theoretically approaches. *Sci Rep* 12 (2022) 18031. <https://doi.org/10.1038/s41598-022-22421-8>
31. J.M. Hofman, D.J. Watts, S. Athey, F. Garip, T.L. Griffiths, J. Kleinberg, H. Margetts, S. Mullainathan, M.J. Salganik, S. Vazire, A.Vespignani, T. Yarkoni, Integrating explanation

and prediction in computational social science, *Nature* 595(2021)181–188.

<https://doi.org/10.1038/s41586-021-03659-0>

32. N.A. El Essawy, A.H. Konsowa, M. Elnouby, H.A. Farag, A novel one-step synthesis for carbon-based nanomaterials from polyethylene terephthalate (PET) bottles waste, *Journal of the Air & Waste Management Association*, 67(2017)358-370.  
<https://doi.org/10.1080/10962247.2016.1242517>
33. M.H. Gouda, S.M. Ali, S.S. Othman, S.A. Abd Al-Aziz, M.M. Abu-Serie, N.A. Elsokary, N.A. Elessawy, Novel scaffold based graphene oxide doped electrospun iota carrageenan / polyvinyl alcohol for wound healing and pathogen reduction: in-vitro and in-vivo study, *Sci Rep.* 11 (2021) 20456. <https://doi.org/10.1038/s41598-021-00069-0>
34. N.A. Elessawy, M.H. Gouda, M. Elnouby, S.M. Ali, M. Salerno, M.E. Youssef, Sustainable microbial and heavy metal reduction in water purification systems based on PVA/IC nanofiber membrane doped with PANI/GO, *Polymers* 14(2022) 1558.  
<https://doi.org/10.3390/polym14081558>
35. A. Tkatchenko, M.Scheffler, Accurate molecular van der Waals interactions from ground-state electron density and free-atom reference data, *Phys Rev Lett* 102(2009) 6–9.  
<https://doi.org/10.1103/PhysRevLett.102.073005>
36. D.S. El-Sayed, Electronic band structure and density of state modulation of amphetamine and ABW type–zeolite adsorption system: DFT-CASTEP analysis, *J Mol Model* 29 (2023) 96. <https://doi.org/10.1007/s00894-023-05501-y>
37. S. Baachaoui, S. Aldulaijan, L. Sementa, A. Fortunelli, A. Dhouib, N. Raouafi, Density Functional Theory Investigation of Graphene Functionalization with Activated Carbenes and

- Its Application in the Sensing of Heavy Metallic Cations, *J. Phys. Chem. C* 125 (2021) 26418–26428. <https://doi.org/10.1021/acs.jpcc.1c07247>
38. G. Box, D.W. Behnken, Some new three level designs for the study of quantitative variables, *Technometrics*. 2(1960) 455–475. <https://www.jstor.org/stable/1266454>
39. M.H. Gouda, N.A. Elessawy, M. Elnouby, M. Ghorab, I.O. Radwan, A. Hashim, M.E. Youssef, D.M.F. Santos, Evaluation of sulfonated chitosan-g-sulfonated polyvinyl alcohol/polyethylene oxide/sulfated zirconia composite polyelectrolyte membranes for direct borohydride fuel cells: Solution casting against the electrospun membrane fabrication technique, *Frontiers in Materials* 9 (2022). <https://doi.org/10.3389/fmats.2022.912006>
40. N. Elessawy, M. Abdel Rafea, N. Roushdy, M. Youssef, M.H. Gouda, Development and evaluation of cost-effective and green Bi-functional nickel oxide decorated graphene electrocatalysts for alkaline fuel cells, *Results in Engineering* 17 (2023)100871. <https://doi.org/10.1016/j.rineng.2022.100871>
41. W.Wan,Z. Zhao, H. Hu, Y. Gogotsi, J. Qiu, Highly controllable and green reduction of graphene oxide to flexible graphene film with high strength, *Mater. Res. Bull.* 48 (2013) 4797-4803. <https://doi.org/10.1016/j.materresbull.2013.08.031>
42. Y. Zhu, Y. Ming, H. Xiao, C. Zhang, J. Wang, Y. Duan, B. Wang, Green synthesis of highly aligned reduced graphene oxide films with competitive performance assisted by sandwiching restriction, *Diamond and Related Materials*. 127(2022) 109166. <https://doi.org/10.1016/j.diamond.2022.109166>
43. D. Khalili, Graphene oxide: a promising carbocatalyst for the regioselective thiocyanation of aromatic amines, phenols, anisols and enolizable ketones by hydrogen peroxide/KSCN in water, *New J. Chem.*, 40 (2016) 2547-2553. <https://doi.org/10.1039/C5NJ02314A>.

44. F.V. Ferreira, F.S. Brito, W. Franceschi, E.A.N. Simonetti, L.S. Cividanes, M. Chipara, K. Lozano, Functionalized graphene oxide as reinforcement in epoxy based nanocomposites, *Surfaces and Interfaces* 10 (2018) 100-109. <https://doi.org/10.1016/j.surfin.2017.12.004>
45. K.R. Balaji, R. Hardian, V.G.D. Kumar, R.Viswanatha, S. Kumar, S. Kumar,A. Singh, M.S.Santosh, G. Szekely, Composite nanofiltration membrane comprising one-dimensional erdite, two-dimensional reduced graphene oxide, and silkworm pupae binder, *Materials Today Chemistry* 22(2021)100602. <https://doi.org/10.1016/j.mtchem.2021.100602>
46. N.A. Elesawy, M.H. Gouda, M. Elnouby,N.A.Taha, M.E. Youssef, D.M.F. Santos, Polyvinyl alcohol/ polyaniline/ carboxylated graphene oxide nanocomposites for coating protection of cast iron in simulated seawater, *Polymers* 14 (2022) 1791. <https://doi.org/10.3390/polym14091791>
47. P. Maziarka, P. Sommersacher, X. Wang, N. Kienzl, S. Retschitzegger, W. Prins, N. Hedin, F. Ronsse, Tailoring of the pore structures of wood pyrolysis chars for potential use in energy storage applications, *Applied Energy*. 286 (2021) 116431. <https://doi.org/10.1016/j.apenergy.2020.116431>
48. Y. Zhang, Z. Chen, L. Yao, X. Wang, Q. M. Fu, Z. D. Lin, S. G. Wang, Study of ion permeation through the graphene oxide/polyether sulfone membranes, *ChemElectroChem* 7 (2020) 493. <https://doi.org/10.1002/celec.201902108>
49. B.M. Ganesh, A.M. Isloor, A.F. Ismail, Enhanced hydrophilicity and salt rejection study of graphene oxide-polysulfone mixed matrix membrane, *Desalination* 313 (2013) 199–207. <https://doi.org/10.1016/j.desal.2012.11.037>
50. G.S. Prihandana, I. Sanada,H. Ito, M. Noborisaka, Y. Kanno, T. Suzuki, N. Miki, Antithrombogenicity of fluorinated diamond-like carbon films coated nano porous poly-

ethersulfone (PES) membrane, *Materials*. 6 (2013) 4309-4323.

<https://doi.org/10.3390/ma6104309>

51. J. Fito, M. Abewaa, A. Mengistu, K. Angassa, A.D. Ambaye, W. Moyo, T. Nkambule, Adsorption of methylene blue from textile industrial wastewater using activated carbon developed from *Rumex abyssinicus* plant, *Sci Rep* 13 (2023)5427.

<https://doi.org/10.1038/s41598-023-32341-w>

52. Y. Han, Z. Xu, C. Gao, Ultrathin graphene nanofiltration membrane for water purification, *Adv. Funct. Mater.* 23 (2013) 3693–3700. <https://doi.org/10.1002/adfm.201202601>

53. Y. Yuan, X. Gao, Y. Wei, X. Wang, J. Wang, Y. Zhang, C. Gao, Enhanced desalination performance of carboxyl functionalized graphene oxide nanofiltration membranes, *Desalination*, 405 (2017)29-39. <https://doi.org/10.1016/j.desal.2016.11.024>

54. M. Khansanami, A. Esfandiari, High flux and complete dyes removal from water by reduced graphene oxide laminate on Poly Vinylidene Fluoride/graphene oxide membranes, *Environmental Research* 201 (2021) 111576. <https://doi.org/10.1016/j.envres.2021.111576>

55. D.A. Gkika, V. Karmali, D.A. Lambropoulou, A.C. Mitropoulos, G.Z. Kyzas, Membranes coated with graphene-based materials: A review, *Membranes* 13 (2023) 127. <https://doi.org/10.3390/membranes13020127>

56. S.I Voicu, V.K. Thakur, Graphene-based composite membranes for nanofiltration: performances and future perspectives, *emergent mater.* 5 (2022) 1429–1441. <https://doi.org/10.1007/s42247-021-00291-6>

57. H. Kwon, Y. Park, E. Yang, T.H. Bae, Graphene oxide-based membranes intercalated with an aromatic crosslinker for low-pressure nanofiltration, *Membranes*. 12(2022)966. <https://doi.org/10.3390/membranes12100966>

58. X.Z. Wei, Z.Q. Gan, Y.J. Shen, Z.L. Qiu, L.F. Fang, B.K. Zhu, Negatively-charged nanofiltration membrane and its hexavalent chromium removal performance, *J. Colloid Interface Sci.* 553(2019) 475–483. <https://doi.org/10.1016/j.jcis.2019.06.051>
59. L. Zhang, R. Zhang, M. Ji, Y. Lu, Y. Zhu, J. Jin, Polyamide nanofiltration membrane with high mono/divalent salt selectivity via pre-diffusion interfacial polymerization, *J. Membr. Sci.* 2021, 636, 119478. <https://doi.org/10.1016/j.memsci.2021.119478>
60. N.S. Suhalim, N. Kasim, E. Mahmoudi, I.J. Shamsudin, A.W. Mohammad, F.M. Zuki, N.L. Jamari, Rejection mechanism of ionic solute removal by nanofiltration membranes: An overview, *Nanomaterials* 12(2022)437. <https://doi.org/10.3390/nano12030437>
61. M. Gouda, N. Elessawy, T. Toghan, Development of hybrid green nanocomposite polymeric beads doped with nano sulfated zirconia for effective removal of Cefotaxime antibiotic from aqueous solution, *Sci Rep* 12 (2022) 12701. <https://doi.org/10.1038/s41598-022-16473-z>
62. J. Luo, Y. Wan, Effects of pH and salt on nanofiltration a critical review, *Journal of Membrane Science.* 438(2013)18–28. <https://doi.org/10.1016/j.memsci.2013.03.029>
63. T. Fujioka, S.J. Khan, J.A. McDonald, L.D. Nghiem, Nanofiltration of trace organic chemicals: A comparison between ceramic and polymeric membranes, *Sep. Purif. Technol.* 136 (2014) 258–264. <https://doi.org/10.1016/j.seppur.2014.08.039>
64. M. Zhu, Y. Liu, M. Chen, D. Gan, M. Wang, H. Zeng, M. Liao, J. Chen, W. Tu, W. Niu, Ultrahigh flux of graphene oxide membrane modified with orientated growth of MOFs for rejection of dyes and oil-water separation, *Chinese Chemical Letters* 31(2020)2683-2688. <https://doi.org/10.1016/j.ccllet.2020.04.011>

65. M.D. Afonso, M.N. de Pinho, Transport of  $MgSO_4$ ,  $MgCl_2$ , and  $Na_2SO_4$  across an amphoteric nanofiltration membrane, *J. Membr. Sci.*, 179 (2000)137-154.  
[https://doi.org/10.1016/S0376-7388\(00\)00495-6](https://doi.org/10.1016/S0376-7388(00)00495-6)
66. G. Moradi, R. Heydari, S. Zinadini, M. Rahimi, A.A. Zinatizadeh, F. Gholami, Fouling alleviation and enhanced salt rejection in NF membranes via incorporation of 5-amino-1-phenyl-3-(thiophen-2-yl)-1H-pyrazole-4 carbonitrile functionalized pectin in PES matrix, *J. Water Process. Eng.*, 48 (2022)102888. <https://doi.org/10.1016/j.jwpe.2022.102888>
67. Y. Zhang, Y. Guo, W. Wan, G. Pan, H. Yu, W. Du, H. Shi, M. Zhao, G. Zhao, C. Wu, Y. Liu, Tailoring molecular structure in the active layer of thin-film composite membrane for extreme pH condition, *J Polym Res* 29 (2022)308. <https://doi.org/10.1007/s10965-022-03155-7>
68. S. Kumari, V.D. Rajput, T. Minkina, P. Rajput, P. Sharma, A.K. Verma, S. Agarwal, M.C. Garg, Application of RSM for bioremoval of methylene blue dye from industrial wastewater onto sustainable walnut shell (*Juglans regia*) biomass, *Water* 2022, 14, 3651.  
<https://doi.org/10.3390/w14223651>
69. M. Chenna, M. Kebaili, N. Lardjane, N. Drouiche, H. Lounici, Modeling and Optimization by RSM for the Removal of the Dye "Palanil blue R" by Coagulation-Flocculation Process, *Int J Environ Res* 16 (2022) 35. <https://doi.org/10.1007/s41742-022-00413-w>
70. S. Shojaei, S. Shojaei, S.S. Band, A.A.K. Farizhandi, M. Ghoroghi, A. Mosavi, Application of Taguchi method and response surface methodology into the removal of malachite green and auramine-O by NaX nanozeolites, *Sci Rep* 11 (2021) 16054. <https://doi.org/10.1038/s41598-021-95649-5>

71. S. Yadav, I. Ibrar, A. Altaee, A.K. Samal, R. Ghobadi, J. Zhou, Feasibility of Brackish Water and Landfill Leachate Treatment by GO/MoS<sub>2</sub>-PVA Composite Membranes, *Sci. Total Environ.* 745 (2020) 141088. <https://doi.org/10.1016/j.scitotenv.2020.141088>
72. P. Xu, J. Hong, X. Qian, Z. Xu, H. Xia, Q.-Q. Ni, “Bridge” graphene oxide modified positive charged nanofiltration thin membrane with high efficiency for Mg<sup>2+</sup>/Li<sup>+</sup> separation, *Desalination* 488 (2020) 114522. <https://doi.org/10.1016/j.desal.2020.114522>.
73. J. Xue, J. Shen, R. Zhang, F. Wang, S. Liang, X. You, Q. Yu, Y. Hao, Y. Su, Z. Jiang, High-flux nanofiltration membranes prepared with  $\beta$ -cyclodextrin and graphene quantum dots. *J. Membr. Sci.* 612 (2020) 118465. <https://doi.org/10.1016/j.memsci.2020.118465>